Expression Profiling of Contralateral Dorsal Root Ganglia of a Rat Model of Complex Regional Pain Syndrome Type-i Uncovers Potential Mechanisms Involved in Mirror-image Painexpression Profiling of Contralateral Dorsal Root Ganglia of a Rat Model of Complex Regional Pain Syndrome Type-i Uncovers Potential Mechanisms Involved in Mirror-image Pain

Huimin Nie
Zhejiang Chinese Medical University
Boyu Liu
Zhejiang Chinese Medical University
Chengyu Yin
Zhejiang Chinese Medical University
Ruixiang Chen
Zhejiang Chinese Medical University
Jie Wang
Zhejiang Chinese Medical University
Danyi Zeng
Zhejiang Chinese Medical University
Yan Tai
Zhejiang Chinese Medical University
Dongwei He
Hebei Medical University
Boyi Liu (boyi.liu@foxmail.com)
Zhejiang Chinese Medical University https://orcid.org/0000-0001-9870-4548

Research

Keywords: RNA-Seq, Pain, CRPS-I, Dorsal root ganglia, Inflammation, Cytokine

Posted Date: May 26th, 2021

DOI: https://doi.org/10.21203/rs.3.rs-532136/v1

Abstract

Background: Mirror-image pain (MIP), which develops from the healthy body region contralateral to the actual injured site, is a mysterious pain phenomenon accompanying many chronic pain conditions, including complex regional pain syndrome (CRPS). However, the pathogenesis of MIP still remained largely unknown. The purpose of this study is to perform an expression profiling to identify genes related with MIP in an animal model of CRPS-I.

Methods: We established a rat chronic post-ischemic pain (CPIP) model to mimic human CRPS-I. RNA-sequencing (RNA-Seq), bioinformatics, qPCR, immunostaining and animal behavioral assays were used to screen potential genes in contralateral dorsal root ganglia (DRG) that may be involved in MIP.

Results: The CPIP model rats developed robust and persistent MIP in contralateral hind paws. Bilateral DRG neurons did not exhibit obvious neuronal damage. RNA-Seq of contralateral DRG from CPIP model rats identified a total 527 differentially expressed genes (DEGs) *vs*. control rats. The expression changes of several representative DEGs were verified by qPCR. Bioinformatics analysis indicated that immune system process, innate immune response and cell adhesion were among the mostly enriched biological processes, which are all important processes involved in pain sensitization, neuroinflammation and chronic pain. We further identified DEGs potentially involved in pain mechanisms or enriched in small- to medium-sized sensory neurons or TRPV1-lineage nociceptors. By comparing with published datasets summarizing genes enriched in pain mechanisms, we sorted out a core set of genes which might contribute to nociception and pain mechanism in MIP.

Conclusions: We provided by far the first study to profile gene expression changes and pathway analysis of contralateral DRG for investigating MIP mechanisms. This work may provide novel insights into understanding the mysterious mechanisms underlying MIP.

Introduction

Mirror-image pain (MIP) is a mysterious pain phenomenon which is accompanied with many clinical pain conditions [1]. MIP develops from the healthy body region which is contralateral to the actual injured site [1–3]. MIP is typically characterized by increased mechanical hypersensitivity on the uninjured mirror-image body side [4]. It can be triggered in response to light touch/pressure stimuli, which are normally perceived as innocuous. Patients with chronic pain, such as complex regional pain syndrome (CRPS) and atypical facial pain, etc. can develop MIP to the unaffected body side.

Complex regional pain syndrome type-I (CRPS-I) is a chronic pain condition that usually impacts the extremities of the patients [5]. It is usually triggered by an initial injury, including tissue ischemia, fractures or surgery in the extremity and develops into a chronic pain condition that impacts the life quality of the patients [6–8]. One of the features of CRPS-I is the MIP developed in the unaffected extremities [9–11]. CRPS-I patients developed hypersensitivity to capsaicin, thermal, and mechanical stimuli in the

unaffected extremities [10]. Furthermore, we and others also observed thermal and mechanical hypersensitivity in the unaffected hind limb of a rat model of CRPS-I [12–16].

At present, the pathogenesis of MIP still remained largely unknown. However, certain possible mechanisms have been proposed to contribute to MIP [17]. Spinal glial activation has been observed in contralateral dorsal horn of MIP model animals [13, 15, 18]. Pharmacological blocking spinal glia metabolism and proinflammatory cytokines (including TNF-α, IL-1β and IL-6) significantly alleviates MIP, suggesting spinal glial and proinflammatory cytokines are involved in MIP [2]. In addition to central mechanism, peripheral mechanisms have also been proposed for MIP. It is reported that TNF-α produced from ipsilateral injured DRG can diffuse to the contralateral side via cerebrospinal fluid and activates satellite cells to produce NGF, which promotes nociceptor excitability on the contralateral side and induce MIP [4]. Although these studies provide evidence suggesting central or peripheral glial and proinflammatory cytokines are important for MIP, it still remains unclear how contralateral DRG is affected in chronic pain conditions and exerts pain signals that may contribute to MIP.

In order to study the molecular mechanisms underlying MIP, we performed a genome-wide expression profiling of DRG innervating the contralateral hind limbs of a rat model of CRPS-I by means of RNA-SEq. We obtained gene expression profiles and identified differentially expressed genes (DEGs) in CPIP model rats *vs*. control rats. We studied the major functions or signaling pathways that these DEGs may be involved in. We further screened the genes which might contribute to nociception and pain processing during MIP. Thus, this study provides novel insights into understanding the peripheral mechanisms contributing to MIP.

Material And Methods

Animals

Male adult Sprague-Dawley rats weighing 300 to 320 g were purchased from Shanghai Laboratory Animal Center, Chinese Academy of Sciences. Rats were randomly assigned to each group and housed in the Laboratory Animal Center of Zhejiang Chinese Medical University accredited by the Association for Assessment and Accreditation of Laboratory Animal Care (AAALAC) under standard environmental conditions (12 h light–dark cycles and 24 ± 2℃). Rats had free access to food and Water. The animals were given one week or so to adapt to the experimental environment before the formal experiment. All animal care and experimental studies were approved by the Laboratory Animal Management and Welfare Ethical Review Committee of Zhejiang Chinese Medical University (Permission Number: ZSLL-2017-183).

CPIP rat model establishment

According to the previous operation, CPIP model was established by prolonged hind paw ischemia and reperfusion [14, 19]. Anesthesia was induced by intraperitoneal injection of 50 mg/kg of sodium pentobarbital and was maintained at a dose of 20 mg/kg/h. Glycerin was applied to the ankle joints of rats. Afterwards, an O-ring rubber with an inner diameter of 7/32 was tightly passed around the right hind

limb just proximal to the ankle joint. The O-ring was cut off 3 hours later or the reperfusion. Control rats received the same anesthesia but a cut O-ring, which could not block blood flow, was applied to the same part.

Determination of mechanical allodynia

Before baseline test, rats were habituated to the testing environment every day for a consecutive 3 days. Rats were individually placed on an elevated mesh floor, covered with transparent Plexiglas chambers. Their feet can be exposed to the eyes of the wire mesh. Rats were habituated for 30 minutes (stop grooming and exploratory activities) before the test. The mechanical hyperalgesia was measured using a series of von Frey filaments (UGO Basile, Italy) applied perpendicularly to the mid-plantar surface of the hind paws, with sufficient force to bend the filament slightly for 5 seconds according to methods we previously used [20]. Nocifensive responses were identified as an abrupt withdrawal of the paw and licking and vigorously shaking in response to the stimulation. The threshold was determined by the “Up-Down” testing paradigm, and the 50% paw withdrawal threshold (PWT) was calculated by the nonparametric Dixon test [21, 22]. Behavior tests were all conducted by an experimenter blinded to experimental conditions.

Measurement of hind paw edema

Edema was observed as an increase in hind paw diameter and measured by a digital caliper, and was calculated as the difference between the basal value and the test value as described in our previous study [13]. Each rat was measured 3 times and the mean value was calculated.

Tissue collection and RNA extraction

At day 7, rats were deeply anesthetized with sodium pentobarbital at a dose of 50 mg/kg and were perfused transcardially with 200 mL 0.9% saline (4℃). After the perfusion, the left (contralateral) side L4-6 DRG segments were collected and were immediately preserved in the RNA later solution (Thermo Fisher, USA). Total RNA was extracted using the Trizol reagent (Thermo Fisher, USA) following the manufacturer’s instructions. DNase I was used to degrade contaminating DNA. The purity and concentration of the samples was assessed by Nanodrop Spectrophotometer (NanoDrop Products, USA) and the RNA integrity was assessed by Agilent 2100 Bioanalyzer (Agilent Technologies, Palo Alto, CA).

Immunofluorescence staining

At day 7, rats were deeply anesthetized with sodium pentobarbital at a dose of 50 mg/kg and were perfused transcardially with 200 mL 4% formaldehyde after 200 mL 0.9% saline (4°C). The bilateral L4-6 DRGs was harvested and post-fixed in the same fixative for 4 h (4°C) before transferring to 15% and 30% sucrose for 48 h for dehydration. A few days later, the DRG were serially cut into 8-μm thick transverse sections on a frozen microtome (Thermo NX50, USA) and mounted on adhesive slides as 8 sets of every 10th serial sections. All the slides were blocked with 5% normal donkey serum in PBS for 1 h at 37°C and then incubated overnight at 4°C with corresponding primary antibodies. The primary antibodies used were rabbit anti-ATF3 (#HPA001562, Sigma) and mouse anti-NeuN (#ab104224, Abcam). The second

day, the sections were rinsed with PBS and incubated for 1 h with a mixture of corresponding secondary antibodies. Nikon A1R laser scanning confocal microscope (Nikon, Japan) was used to capture fluorescence images. Uniform microscope settings were maintained throughout all image capture sessions in order to quantitative fluorescence intensity analysis. All stained sections were examined and analyzed in a blinded manner. Five images were randomly selected per rat tissue and averaged. Then compared according to methods described in our previous studies.

RNA-Seq library establishment and RNA-Seq

We isolated the total mRNAs of 4 rats of each group and used them to construct sequencing libraries. mRNA were purified from total RNA using oligo (dT)-attached magnetic beads using two rounds of purification. Following purificatio, mRNA was fragmented into small pieces using fragmentation reagent under elevated temperature. Subsequently, first-strand cDNA was generated by random hexamer-primed reverse transcription, followed by a second-strand cDNA synthesis. The synthesized cDNA was subjected to end-repair and then was 3’ adenylated. Adaptors were ligated to the ends of these 3’ adenylated cDNA fragments. This process is to amplify the cDNA fragments with adaptors from previous step. PCR products are purified with the SPRI beads and dissolved in EB solution. The double stranded PCR products were heat denatured and circularized by the splint oligonucleotide sequence. The single-strand circle DNA (ssCir DNA) was formatted as the final library. Library was validating on the Agilent Technologies 2100 bioanalyzer. The DNA nanoballs were loaded into the patterned nanoarray and single-end 50 base reads were generated in the way of sequenced by synthesis. Finally, the fragments were enriched by PCR amplification to construct a library ready for sequencing using BGI SEQ-500 by BGI Group (Shenzhen, China).

Bioinformatics analysis

Primary sequencing data produced by RNA-Seq (raw reads) were subjected to quality control (QC). The information of total reads and mapping ratio reads were shown in Table 1. Raw reads were filtered into clean reads using internal software SOAP nuke (version 1.5.2), as follows: Remove reads in which unknown bases (N) are more than 10%; Remove reads with adaptors; Remove low quality reads (we define the low quality read as the percentage of base which quality is < 15 and > 50% in a read). QC of alignment was performed to determine if re-sequencing was needed. If the alignment result passed QC, downstream analysis including gene expression, differentially expressed genes, cluster analysis, Gene Ontology (GO) enrichment analysis, Kyoto Encyclopedia of Genes and Genomes (KEGG) pathway enrichment analysis and Gene Set Enrichment Analysis (GSEA) analysis were then performed.

Table 1
Sequences of the primers used for qPCR validation of RNA-Seq data.

Gene name	Gene ID	Primer sequence (5' -3')	Amplicon size (bp)
Gpr183	679975	F: 5’-GCAGAACCCACTGACCGAGAAATC-3’	83
Tlr8	684440	R: 5’-ACAAGACGAACACGCCGATGATG-3’	142
Tbx18	315870	F: 5’-CGCCTTGACCGTCTGTGGAATG-3’	98
Egfr	24329	R: 5’-GGCTCTGAGGCAAGTTGAGGAATG-3’	145
Cxcl13	498335	F: 5’-GCAAGGCAACACAAGTTCTTCAGC-3’	219
Slfn1	688900	R: 5’-GAGAGGAACAGGAGGAGCCAGAC-3’	113
Gli2	304729	F: 5’-CACTACGCCGCCTGCTTCAAG-3’	144
Stk32b	305431	R: 5’-ACTGTGCCAAATGCTCCTGAACC-3’	96
Asgr2	29403	F: 5’-CGACTTTGAAAGGTTGCTTGTA-3’	136
Smoc2	292401	R: 5’-ACACTGGATGAATAGGAAACGT-3’	117
Fcgr1a	295279	F: 5’-GCTGAGAGTGACCACAGGCATTG-3’	140
Osr2	315039	R: 5’-AGCCCAAGACAGACTCCCACAG-3’	139
Sned1	316638	F: 5’-ACCTCCATCACCGTGCCTACC-3’	89
Siglec1	311426	R: 5’-AGTCTTGACCTTGCTCCGCTTATG-3’	119
Myl1	56781	F: 5’-AGAAGTGCGTGGAGAGGGATGAG-3’	103
Myom2	306616	R: 5’-AGTACCACAGGTTCACCAGGAAGG-3’	107
Capg	297339	F: 5’-CACGGAGGTAGCAGGAATGACAAC-3’	97
Retsat	246298	R: 5’-AGGTCAGGGTTCGCAGATCCAG-3’	128
		F: 5’-AGGAAGCCAAGCAACCCAAGAATG-3’	
		R: 5’-CTACCAGCACACACCAGCAGTATC-3’	
		F: 5’-CCTGGCTTACGGCTTTACTTCTCC-3’	
		R: 5’-CCGTCCTCCGTGGCTACCTC-3’	
		F: 5’-CGGCAAAGTGTTCAGGCGAAAC-3’	
		R: 5’-TGGAAGGCGTGGAGAGGTGTC-3’	
		F: 5’-CTGCGTCCGTGCCTCAATGG-3’	
		R: 5’-GTGAAGCCAGCGAGACAGGAAC-3’	
		F: 5’-ACTCCAGACCTGACCACCTTCTTG-3’	
		R: 5’-GCCAATGTGAGACCTCCGTGTG-3’	

Gene name	Gene ID	Primer sequence (5' -3')	Amplicon size (bp)
		F: 5’-AGCAGACTGAGAGGAGCAGGAAG-3	
		R: 5’TTGGTGTTGATGAGGCTGGTGTTC-3	
		F: 5’-AAGACAACCACCAACGCTCACTG-3’	
		R: 5’-GCCACGATTCTTCTCAGCAAATGC-3’	
		F: 5’-GGAGAGGAGCCAGCCGAGATG-3’	
		R: 5’-CGTTGGTCTGGTCCGCTGTAATG-3’	
		F: 5’-GAGCGTGCGGTGTCAGTGTG-3’	
		R: 5’-TGGCAGGTAGCGGACAGACTC-3’	

Cluster analysis and screening of differentially expressed genes

Distances of expressed genes were calculated using the Euclidean method [23]. The sum of the squared deviations algorithm was used to calculate distance. The cluster analysis and heat map visualization of gene expression patterns was performed using the “pheatmap” package in the R software of Bioconductor. Differentially expressed mRNAs with statistical significance were identified through Volcano Plot filtering. The threshold required for the results to be considered significant was as follows: q-value ≤ 0.001 and fold change ≥ 1.5 or ≤ 0.667.

Functional enrichment analysis of DEGs

Functional enrichment analysis was performed through functional annotation package “cluster Profiler” in R studio software (RStudio, Boston, MA, USA). GO and KEGG enrichment analysis were also conducted. For each enriched function term, Q-value of enriched functions and the Q-value by multiple testing corrections were calculated by “cluster Profiler” package in R studio software. The GO functional and KEGG pathway enrichment analysis were performed for DEGs using the Database for Annotation, Visualization and Integrated Discovery (DAVID) online tools (http://www.geneontology.org and http://www.genome.jp/kegg).

GSEA analysis

Gene set enrichment analysis (GSEA) was performed according to methods previously described [24]. We chose the top 10 most significantly upregulated pathways from GSEA analysis. The gene sets were downloaded from the Molecular Signatures Database v7.1 (https://www. gsea-msigdb.org/gsea/msigdb/index.jsp). A FDR ≤ 0.25 and NES 1.0 were adopted as the criterion for judging significance [24].

Real-time quantitative PCR (qPCR) analysis

According to the manufacturer's instruction, the extracted total RNA from the DRGs was reverse transcribed into cDNA using random hexamers primers (TaKaRa Bio Inc., Shiga, Japan). The sequences of all primers used were shown in Table 1. qPCR was performed using the LightCycler® 480 SYBR Green I Master (Roche America) 20 μL reaction system according to the manufacturer's protocol by LightCycler480 System (Roche, America). Each reaction was performed in triplicates and normalized to β-actin gene expression. The CT value of each well was determined using the LightCycler480 System software and the average of the triplicates was calculated. The relative quantification was determined by the △△CT method [25, 26].

Source of microarray data

Pain genes (PG): The pain gene list was retrieved from a previous study using the same list to predict potential genes related to mediating masseter inflammation-induced pain [27]. This pain gene list contains 685 genes, which mainly includes central and peripheral inflammatory responses and pain mood and affect, human genes related to transmission of pain signals (see Suppl. Table 1 for full list of genes).

Sensory neuronal genes (SN): The sensory neuronal gene list was retrieved from a previous study by magnetic cell sorting (MACS) to separate neuronal cells from nonneuronal cells from mouse DRG [28]. According to this study, MACS successfully segregated neuronal cells from non-neuronal cells from mouse DRGs. This procedure can enrich neuronal population up to 95% compared with 10% before sorting. Transcriptome analysis further confirmed that a lot of genes were enriched in the neuronal population collected through MACS. We selected genes that showed increase in expression by > 40% according to criterion described by Chung et al. [27] (see Suppl. Table 2 for full list of genes).

TRPV1-lineage neuronal genes (VL): TRPV1-lineage neuronal genes list was retrieved from a study which identified a group of genes enriched in TRPV1 expressing nociceptive sensory neurons [29]. By using mouse lines selectively labeling or ablating TRPV1 lineage neurons, Goswami et al. identified a group of genes enriched in VL sensory neurons. We screened genes that are enriched > 3-fold in VL neurons compared to non-VL neurons according to a study by Chung et al. [27] (see Suppl. Table 3 for full list of genes).

Protein-protein interaction (PPI) network analysis

The Search Tool for the Retrieval of Interacting Genes (STRING) is used to provide information regarding predicted and experimental interactions of proteins and the prediction method of this database is from neighborhood, gene fusion, co-occurrence, co-expression experiments, databases, and text mining. By setting the Combination score > 0.7 as the reliability threshold value, the web based STRING database (http:// string-db.org/) was used to produce PPI predictions after uploading the union gene list to the search bar [30]. Based on the interplayed relationships, a PPI network was established and then visualized using the Cytoscape software [31]. The connectivity degree of each protein, namely the number of proteins it connected, was calculated to evaluate its importance in this network.

Statistical analysis

Data in graphs are expressed as means ± SEM. One- or two-way ANOVA followed by Tukey's post hoc test was used for comparisons among groups ≥ 3. Student's *t* test was used for comparisons between two groups. The comparison is considered significantly different if the *p*-value is less than 0.05.

Results

1. The establishment of a rat model of CRPS-I and evaluation of the nocifensive behavior

We first established the rat CPIP model to mimic human CRPS-I following methods described before [14, 19]. An O-ring with 7/32 internal diameter was tightly passed around the right hind limb just proximal to the ankle joint and applied for 3 h. During the ligation, the right hind limb displayed obvious cyanosis (an indication of tissue hypoxia) and edema (Fig. 1A). The edema persisted 3 days and gradually returned back to normal (Fig. 1B&C). The PWT (paw withdrawal threshold) of ipsilateral hind paws of CPIP model group rats was significantly reduced on Day 1 compared with control group and lasted over 7 days (Fig. 1D&F) Moreover, the contralateral hind paw also showed significant reduction in PWT on Day 1 compared with control rats and persisted over 7 days (Fig. 1E&G). These results were consistent with previous studies [13–15], demonstrating the presence of MIP in CPIP model rats.

2. Pathological evaluation of ipsilateral and contralateral DRG neurons innervating the hind paws

We sacrificed the rats on Day 7 and harvested bilateral L4-6 DRG. We first performed immunostainings to examine whether there was any neuronal damage occurred in DRG. We used ATF3, a widely used marker for neuronal damage for the examination. As shown in Fig. 2A-C, we did not identify any ATF3 positively stained neurons in ipsilateral or contralateral L4-6 DRG of CPIP model rats compared with control rats. For positive control, in one of our recent studies, we stained DRGs with ATF3 from paclitaxel-treated rats, a rat model for chemotherapy-induced peripheral neuropathy and well known for its peripheral neuropathy. We found the number of ATF3 positively expressed neurons was significantly increased in DRG of paclitaxel-treated rats *vs*. control rats [32]. Therefore, the above results indicated no neuronal damage occurred in bilateral DRG neurons of the CPIP model rats.

3. Examination of gene expression profile changes in contralateral DRG from CPIP model rats via RNA-Seq

To gain further insights into the mechanisms underlying MIP of CPIP model rats, we harvested contralateral L4-6 DRG at Day 7 from CPIP model and control rats and analyzed the gene expression profiles via RNA-SEq. We managed to obtain high quality RNA for RNA-Seq analysis (Suppl. Figure 1). RNA-Seq generated approximately 23.9 million raw reads from each sample. The ratio of clean reads reached above 98.0% (Table 2). Over 90% of bases had a quality score ≥ Q30 and over 94% of the clean

reads were mapped to rat genome. In all, a total of 23, 267 genes were successfully mapped and identified from RNA-Seq (Suppl. Table 4). We then filtered out the differentially expressed genes (DEGs) with the criteria of fold change ≥ 1.5 or ≤ 0.667 and *q*-value ≤ 0.001 (Suppl. Table 5). We displayed the DEGs of CPIP group *vs*. control group in the volcano plot as shown in Fig. 3A. In all, 527 DEGs (including 245 up- and 282 down-regulated) were identified from CPIP group *vs*. control group (Fig. 3A). We further summarized and plotted the identified DEGs in a heat map as shown in Fig. 3B. The cluster analysis indicated a high level of consistency within CPIP or control group samples but a clear separation between these two groups (Fig. 3B).

Table 2
The information of total reads and mapping ratio for Sham and CPIP groups in RNA-Seq.

Sample	Total Raw Reads (M)	Total Clean Reads (M)	Clean Reads Q30 (%)	Clean Reads Ratio (%)	Total Mapping (%)
CPIP1	23.92	23.74	93.65	99.22	94.65
CPIP2	23.92	23.74	93.86	99.21	94.83
CPIP3	23.92	23.73	93.96	99.2	94.81
CPIP4	23.92	23.74	93.15	99.24	94.47
Con1	23.92	23.66	93.21	98.88	94.08
Con2	23.92	23.73	94.01	99.19	94.75
Con3	23.92	23.73	93.59	99.2	94.66
Con4	23.92	23.75	93.58	99.27	94.71

4. Analysis of DEGs from contralateral DRGs of CPIP model rats

Among the DEGs we identified, a certain number of genes were reported to participate in pain mechanisms, which include: *Cxcl14* (C-X-C motif chemokine 14 precursor, fold change = 3.2), *Cxcl13* (C-X-C motif chemokine 13 precursor, fold change = 2.6), *Tlr5* (Toll-like receptor 5, fold change = 2.6), *Ngf* (Nerve growth factor, fold change = 2.3) and *Tlr8* (Toll-like receptor 8, fold change = 1.8). We further analyzed the RNA-Seq data and identified 167 genes (63 up-regulated and 104 down-regulated gene) showing expression changes > 10-fold, including *Tsr2* (TSR2 Ribosome Maturation Factor, fold change = 109,177.8), *Aph1b* (Gamma-Secretase Subunit APH-1B, fold change = 436.9), etc. 124 genes had expression changes between 5- and 10-fold, including 40 up-regulated and 84 down-regulated genes. The top 20 up- or 20 down-regulated DEGs was summarized in Table 3&4.

Table 3
The detailed information of the top 20 upregulated DEGs

Upregulated Gene	Gene ID	Location	log_2 fold-change (CPIP/Sham)	Q value	Official gene name (NCBI)
Tsr2	317418	4:20141406–20146082	16.73631777	3.05E-48	TSR2, 20S rRNA accumulation, homolog (S. cerevisiae)
LOC100912618	100912618	4:5867350–5869085	10.69826964	1.77E-12	ubiquitin-conjugating enzyme E2 variant 1-like
LOC100910581	100910581	4:21987993–21989200	9.114037693	6.00E-51	protein phosphatase 1 regulatory subunit 35-like
Aph1b	300802	4:72508008–72598921	8.771010005	5.97E-42	aph-1 homolog B, gamma secretase subunit
LOC103691556	103691556	4:144191722–144211986	7.608251098	8.58E-60	mothers against decapentaplegic homolog 9
LOC102550456	102550456	4:21748602–22021862	7.14204003	4.65E-16	TSC22 domain family protein 4-like
LOC108349606	108349606	4:166282044–166282845	6.69115347	3.43E-12	60S ribosomal protein L7a-like
LOC100911233	100911233	4:33876697–33909836	6.417167166	2.65E-10	cell division cycle and apoptosis regulator protein 1-like
LOC100912399	100912399	4:43938500–44000199	6.383284264	4.34E-10	mitogen-activated protein kinase kinase kinase 1-like
Potef	684969	4:24780521–24783147	6.285874308	1.68E-09	POTE ankyrin domain family, member F
Hmgn5	100910616	4:80134557–80142902	5.972626604	7.99E-08	high mobility group nucleosome binding domain 5
LOC108348106	108348106	4:90957132–90962541	5.585249332	3.78E-06	alpha-ketoglutarate-dependent dioxygenase alkB homolog 6
LOC100909795	100909795	4:16314107–16317575	5.500305695	7.81E-06	colorectal mutant cancer protein-like
LOC100911564	100911564	4:71676810–71681062	5.395697586	1.82E-05	glycine N-methyltransferase-like
LOC100361265	100361265	4:94827988–94840706	5.30501238	1.26E-09	
RGD1584023	690146	4:116933277–116936466	5.00539585	2.68E-04	
RGD1560795	297402	4:134996–135398	4.968015878	3.36E-04	
LOC102552708	102552708		4.877490295	5.64E-04	
Zp2	81828		4.462124948		
Slc25a36l1	364991		3.968951847		

Upregulated Gene	Gene ID	Location	log_2 fold-change (CPIP/Sham)	Q value	Official gene name (NCBI)
		4:189899906–189911650		2.03E-05	
		4:37019755–37022003		6.98E-10	rCG64283-like similar to zinc finger protein 11B similar to Sepiapterin reductase (SPR) DNA-directed RNA polymerase II subunit GRINL1A-like zona pellucida glycoprotein 2 solute carrier family 25 (pyrimidine nucleotide carrier), member 36-like 1

Table 4
The detailed information of the top 20 upregulated DEGs

Downregulated Gene	Gene ID	Location	log_2 fold-change (CPIP/Sham)	Q value	Official gene name (NCBI)
LOC100909761	100909761	4:78661643–78681196	-8.814802024	5.59E-86	myotilin-like
Myot	291605	4:35573978–35593541	-8.321037008	2.02E-32	Myotilin
LOC100910177	100910177	4:52919250–52919654	-8.043339285	1.43E-27	dolichol-phosphate mannosyl transferase subunit 3-like
Mb	59108	4:118101633–118108864	-7.245234184	0	myoglobin
Myh2	691644	4:53711895–53738164	-7.020133868	0	myosin heavy chain 2
LOC108348161	108348161	4:52767635–52778693	-6.986899856	1.22E-14	phytanoyl-CoA hydroxylase-interacting protein
LOC103694902	103694902	1:2148–29792	-6.605321706	1.95E-196	ubiquitin-conjugating enzyme E2 B
LOC103690173	103690173	1:3738–18580	-6.475307726	1.07E-10	zinc finger protein 280B-like
LOC100359951	100359951	4:1012044–1012567	-6.336444056	8.02E-10	ribosomal protein S20-like
LOC100909700	100909700	4:81609177–81627763	-6.201682182	4.93E-09	CD177 antigen-like
Txlnb	308622	4:12915781–12961680	-6.187131229	3.36E-34	taxilin beta
Cacng1	29658	4:95921479–95934170	-6.167231672	4.38E-17	calcium voltage-gated channel auxiliary subunit gamma 1
Myl1	56781	4:73937820–73958480	-6.018352729	0	myosin, light chain 1
Nmrk2	100912521	4:11382966–11386170	-5.997306671	5.91E-08	nicotinamide riboside kinase 2
LOC100361543	100361543	4:37261428–37262470	-5.95800371	9.12E-08	RhoA activator C11orf59-like
Myl2	363925	4:39947717–39966734	-5.951502981	9.79E-08	myosin light chain 2
Igfn1	304823	4:52791184–52823037	-5.912190057	7.21E-85	immunoglobulin-like and fibronectin type III domain containing 1
Tnnc2	296369	4:161243606–161246543	-5.911770486	0	troponin C2, fast skeletal type
Ucp3	25708		-5.87994972	3.84E-14	uncoupling protein 3
LOC100911166	100911166		-5.703837223		

Downregulated Gene	Gene ID	Location	log_2 fold-change (CPIP/Sham)	Q-value	Official gene name (NCBI)
		4:165482912–165495895 4:112519789–112524281		1.25E-06	RNA pseudouridylate synthase domain-containing protein 2-like

5. RNA-Seq data validation by means of qPCR

We then set to validate the RNA-Seq data by means of qPCR. We randomly selected 8 up-regulated genes (*Tbx18, Slfn1*, *Gli2*, *Stk32b*, *Asgr2*, *Smoc2*, *Osr2* and *Sned1*) and four down-regulated genes (*Myl1*, *Myom2*, *Capg* and *Retsat*) from the DEGs list and verified their expression by qPCR. The results of qPCR showed that the expression of *Tbx18, Slfn1*, *Gli2*, *Stk32b*, *Asgr2*, *Smoc2*, *Osr2* and *Sned1* were all significantly up-regulated, whereas *Myl1*, *Myom2*, *Capg* and *Retsat* were all significantly down-regulated in contralateral DRG of CPIP model rats *vs*. control rats (Figure 4A&B), which is consistent with RNA-Seq data. We then proceeded to evaluate some typical genes which are reported to contribute to pain or neuroinflammation. These genes include *Gpr183*, *Tlr8*, *Egfr*, *Cxcl13, Fcgr1a* and *Siglec1*. qPCR testing showed that the expression of these genes were all significantly increased in CPIP model rats *vs*. control rats, which is consistent with the RNA-Seq result (Fig. 4C).

6. Function and pathway analysis of DEGs from contralateral DRGs of CPIP model rats

In order to gain more insights into the molecular mechanisms underlying MIP of CRPS-I, gene ontology (GO) enrichment analysis was performed to analyze the DEGs from contralateral DRGs of CPIP model rats *vs*. control rats. GO enrichment analysis indicated that the mostly enriched biological process among up-regulated DEGs included immune system process, innate immune response and cell adhesion, etc. (Figure 5A). The mostly enriched molecular function among up-regulated DEGs included low-density lipoprotein particle binding, carbohydrate binding, and heparin binding, etc. (Figure 5B). The mostly enriched cellular function among up-regulated DEGs included extracellular region and extracellular matrix, etc. (Figure 5C). On the other hand, the mostly enriched biological process among down-regulated DEGs included muscle contraction, sarcomere organization and ossification, etc. (Figure 5D). The mostly enriched molecular function of down-regulated DEGs included actin binding, structural constituent of muscle and actin filament binding, etc. (Figure 5E). The mostly enriched cellular function of down-regulated DEGs included Z disc, myofibril and M band, etc. (Figure 5F). The DEGs allocated to each category of GO analysis are summarized in Suppl. Table 6.

We performed KEGG analysis to analyze the DEGs from contralateral DRG of CPIP model rats. KEGG analysis indicated that the up-regulated DEGs were involved in complement and coagulation cascades, phagosome and osteoclast differentiation, etc. (Figure 6A). In contrast, the down-regulated DEGs were involved in cardiac muscle contraction, apelin signaling pathway and glucagon signaling pathway, etc. (Figure 6B, Suppl. Table 5). We further performed gene set enrichment analysis (GSEA) of the up-regulated DEGs. Suppl. Fig. 2 listed the most significantly enriched pathways of these DEGs (NES > 1.0,

FDR ≤ 0.25), including complement and coagulation cascades and Toll-like receptor signaling pathway, etc.

Next, we aim to focus our analysis more on the genes related with pain processing. We were able to retrieve three datasets that summarized genes enriched in small-diameter primary sensory DRG neurons (SN), TRPV1-lineage nociceptors (VL) and pain-related genes (PG), respectively [27]. We then compared the DEGs we identified from RNA-Seq with these three datasets. We identify that 19 DEGs were related with PG and *Stoml3*, *Fosb* and *Gdnf* are among the genes most up-regulated (Figure 7A, Suppl. Table 7). We identified 4 DEGs were related with SN and *Eno3* showed the most down-regulation (Figure 7A, Suppl. Table 7). We identified 7 genes were related with VL and *Fosb* showed the most up-regulation (Figure 7A, Suppl. Table 7). PPI analysis was conducted on these 26 genes and the major hub genes identified from the network included *Mmp9*, *Egr1*and *Ngf*, etc. (Figure 7B).

7. Comparison of DEGs derived from contralateral DRG with those from ipsilateral DRG in CPIP model rats

In one of our recent studies, we published the RNA-Seq dataset exploring gene expression changes in ipsilateral DRG of CPIP model rats [12]. We then continued to compare the DEGs derived from contralateral DRG with those from ipsilateral DRG in CPIP model rats. We imposed the same criteria (fold change ≥ 1.5 or ≤0.667, q ≤ 0.001) on these two datasets to identify overlapped DEGs. We found that the contralateral DEGs showed an overlapping of 130 genes with ipsilateral DEGs, which takes up 24.7% of DEGs derived from contralateral DRG of CPIP model rats (Fig. 8, Suppl. Table 7).

Discussion

In this study, we established the rat CPIP model to replicate CRPS-I. We found the model rats developed robust MIP in contralateral hind paws. We then performed expression profiling of the DRG innervating the contralateral hind limb of the model rats by RNA-Seq. We identified the DEGs and validated the expression by means of qPCR. We then studied the major functions or signaling pathways that these DEGs are involved in. Lastly, by comparing with published datasets that summarized genes enriched in pain mechanisms, we further sorted out the genes which might contribute to nociception and pain processing. Thus, we provided by far the first study to profile gene expression changes and performed pathway analysis of contralateral DRG for investigating MIP mechanisms.

CRPS-I is a chronic and devastating pain condition that usually affects the extremities of the patients. One feature of CRPS-I patients is the symptom of MIP [9, 10]. CRPS-I patients may develop increased sensitivity to chemical, thermal, and mechanical stimuli in bilateral extremities [10]. In order to facilitate mechanistic studies of CRPS-I, a rat chronic post-ischemic pain (CPIP) model was developed by applying prolonged hind paw ischemia and reperfusion to mimic CRPS-I [14]. The rat CPIP models exhibits several key features that resemble CRPS-I, including early hind paw edema, vascular disturbance and blood flow dysfunction in hind paw, persistent bilateral mechanical allodynia and heat hyperalgesia and increased sensitivity to capsaicin treatment, etc. [13, 14, 19, 33] At present, the CPIP model has become a commonly

used animal model for CRPS-I mechanistic studies. We and others found that the CPIP model rats develop robust MIP symptoms in the unaffected hind paw, including mechanical and thermal hypersensitivities [13-15]. Therefore, in the present study, we established the rat CPIP model and made good use of it for the mechanistic study of MIP.

We first performed a pathological analysis to examine whether there is any neuronal damage occurred in DRG innervating the hind paws of CPIP model rats. Immunostaining showed that the expression of ATF3, a well-established neuronal damage marker, is not altered in ipsilateral or contralateral DRG of CPIP model rats, suggesting bilateral DRG neurons remain intact in CPIP model rats. In an earlier study, Coderre et al. found no evidence of degeneration in bilateral tibial nerves of CPIP model rats [14]. These findings are consistent with clinical definition that CRPS-I patient have no known or identifiable peripheral nerve injury. Thus, this result excludes the possibility that neuronal damage may contribute to MIP in CPIP model rats.

The pathogenesis of MIP still remained largely unknown. Peripheral mechanisms have been proposed to contribute to MIP. For example, in an animal model for neuropathic pain, it is found that TNF-α is produced from ipsilateral injured DRG and diffuses to contralateral side via cerebrospinal fluid. TNF-α then activates satellite cells to produce NGF, which promotes nociceptor excitability on the contralateral side and induce MIP [4]. Although these findings suggested that peripheral satellite glia cells and pro-inflammatory cytokines are important for MIP, it still remains unclear how contralateral DRG is affected during chronic pain conditions and exerts pain signal that contributes to MIP. Therefore, we performed a genome-wide expression profiling of the DRG that innervate the contralateral hind limbs of the rat CPIP model by means of RNA-Seq.

According to GO enrichment analyses of DEGs in contralateral DRG, we found that the mostly enriched biological processes of up-regulated genes were mainly involved in immune system process, innate immune response, cell adhesion, response to lipopolysaccharide and inflammatory response, etc. This information indicates that immune and inflammatory responses, which can cause neuroinflammation, take place in contralateral DRG. This finding is similar with our recent study which identified lipopolysaccharide and inflammatory response as the predominant biological process in ipsilateral DRG of CPIP model rats [12]. It is known that that neuroinflammation, including inflammatory cytokine/chemokine release, glial cell activation and inflammatory cell infiltration in sensory nerve system, make important contributions to the initiation and maintaining phase of chronic pain [34-37]. Therefore, this result suggests that neuroinflammation in contralateral DRG may constitute an important mechanism for MIP of CPIP model rats.

In addition, KEGG pathway analysis indicated that one of the mostly enriched pathways that these DEGs participate in is “phagosome”. This finding is similar with our recent studies showing that phagosome is a major signaling pathway occurred in ipsilateral DRG and spinal cord dorsal horn (SCDH) of CPIP model rats [12, 15]. Similar findings were also reported in SCDH of an animal model of neuropathic pain [38]. *Itgam* is a well-established marker gene for monocytes and microphages and is involved in phagosome

process. In this study, we found that *Itgam* gene expression is significantly up-regulated in contralateral DRG of CPIP model rat by RNA-Seq. This implies that macrophage or monocyte infiltration may take place in contralateral DRG of CPIP model rats. Macrophages or monocytes can infiltrate into peripheral tissues and sensory ganglia, where they release an array of inflammatory cytokines and ROS products [39-42]. These products activate or sensitize peripheral sensory neurons to produce or enhance pain through neuro-immune crosstalk [35]. Therefore, this result suggests that macrophage or monocyte infiltration in contralateral DRG may contribute to the mechanism of MIP in CPIP model rats.

NGF is a neurotrophic factor and neuropeptide implicated in a wide range of development and maintenance functions. NGF can be released upon tissue inflammation and is implicated in chronic pain [43]. NGF sensitizes nociceptors and promotes their excitability by up-regulating TRPV1 and Nav1.8 channel expression and activity via acting on TrkA receptor [44, 45]. In a previous study, Cheng et al. found that TNF-α produced from ipsilateral injured DRG of a rat spinal nerve ligation model can diffuse to contralateral side via cerebrospinal fluid and activates satellite cells to produce NGF, which promotes nociceptor excitability on the contralateral side and induce MIP [4]. This study suggests that NGF expression is up-regulated in contralateral DRG and contributes to MIP. In our study, RNA-Seq identified that *Ngf* gene is significantly up-regulated in contralateral DRG of CPIP model rats, a result consistent with Cheng et al.'s finding. Thus, our result suggests that NGF may be potentially involved in mediating MIP of CPIP model rats.

By means of RNA-Seq and qPCR validation, we found that chemokine *Cxcl13* gene expression showed significant up-regulation in contralateral DRG. CXCL13 is known as a B-cell-attracting chemokine that acts upon its receptor CXCR5 to exert biological functions. Recent studies identified that CXCL13/CXCR5 axis is present in peripheral sensory ganglia and spinal cord and contribute to chronic pain mechanisms [46-48]. Genetic knockout or knockdown of CXCL13/CXCR5 significantly reduced chronic pain as well as glial cell over-activation in SCDH in an animal model of neuropathic pain [48]. Intrathecal CXCL13 injection can provoke thermal and mechanical hypersensitivities in naïve animals [48]. Moreover, it is found that CXCl13 is increased in DRG neurons of CFA-induced inflammatory model mice and acts upon CXCR5 in DRG neurons to activate p38-MAP kinase, which enhances Nav1.8 channel expression and contributes to chronic pain [47]. Therefore, our findings suggest CXCL13 released from contralateral DRG may contribute to MIP of CPIP model rats.

In conclusion, to our knowledge, this is the first study that performs expression profiling of gene changes in contralateral DRG of an animal model of CRPS-I by RNA-Seq to explore MIP mechanisms. This study identifies a number of genes and signaling pathways in contralateral DRG that may possibly contribute to MIP. Thus, this study may provide novel insights into understanding the mysterious mechanisms underlying MIP.

Abbreviations

CRPS-I: Complex regional pain syndrome type-I; MIP: Mirror-image pain; CPIP: Chronic post-ischemic pain; RNA-Seq: RNA-sequencing; qPCR: Real-time quantitative PCR; DRG: Dorsal root ganglia; DEGs: Differentially expressed genes; PWT: Paw withdrawal threshold; QC: Quality control; GO: Gene Ontology; KEGG: Kyoto Encyclopedia of Genes and Genomes; GSEA: Gene set enrichment analysis; PG: Pain genes; SN: Sensory neuronal genes; VL: TRPV1-lineage neuronal genes; PPI: Protein-protein interaction; STRING: Search Tool for the Retrieval of Interacting Genes; BP: Biological processes; MF: Molecular function; CC: Cellular component.

Declarations

Acknowledgements

Not applicable.

AUTHOR CONTRIBUTIONS

HN, DZ, RC, JW, YL, XL, RX, HW and PW performed the experiments and analyzed the data. D H, BL (Boyu Liu) and CY performed bioinformatics analysis. XS. and JF coordinated with model establishment. JF and BL (Boyi Liu) designed and supervised the study. BL (Boyi Liu) wrote the manuscript. All authors reviewed the manuscript. All the authors read and approved the final manuscript.

FUNDING

This project was supported by the National Natural Science Foundation of China (81873365), Zhejiang Provincial Natural Science Funds for Distinguished Young Scholars (LR17H270001), National Natural Science Foundation of China (81603676), Zhejiang Provincial Natural Science Funds (LQ21H270004), research funds from Zhejiang Chinese Medical University (Q2019J01, KC201943), Natural Science Foundation of Hebei Province (H20206360) and Projects from Health and Family Planning Commission of Hebei Province (20201069).

Availability of data and materials

The key data are contained in the figures, tables, and additional files. The datasets used and/or analyzed during this study can be further obtained from the corresponding author on reasonable request.

Ethics approval and consent to participate

All animal care and experimental studies were approved by the Laboratory Animal Management and Welfare Ethical Review Committee of Zhejiang Chinese Medical University (Permission Number: ZSLL-2017-183).

Consent for publication

Not applicable.

Competing interests

The authors declare that there are no competing interests.

References

1. Huang D, Yu B. The mirror-image pain: an unclered phenomenon and its possible mechanism. Neurosci Biobehav Rev. 2010;34(4):528–32.
2. Milligan ED, et al. Spinal glia and proinflammatory cytokines mediate mirror-image neuropathic pain in rats. J Neurosci. 2003;23(3):1026–40.
3. Kambiz S, et al. Mirror-image pain after nerve reconstruction in rats is related to enhanced density of epidermal peptidergic nerve fibers. Exp Neurol. 2015;267:87–94.
4. Cheng CF, et al. Mirror-image pain is mediated by nerve growth factor produced from tumor necrosis factor alpha-activated satellite glia after peripheral nerve injury. Pain. 2014;155(5):906–20.
5. Ott S, Maihofner C. Signs and Symptoms in 1,043 Patients with Complex Regional Pain Syndrome. J Pain. 2018;19(6):599–611.
6. Birklein F, et al. Complex regional pain syndrome - phenotypic characteristics and potential biomarkers. Nat Rev Neurol. 2018;14(5):272–84.
7. Coderre TJ, Bennett GJ. A hypothesis for the cause of complex regional pain syndrome-type I (reflex sympathetic dystrophy): pain due to deep-tissue microvascular pathology. Pain Med. 2010;11(8):1224–38.
8. Urits I, et al. Complex Regional Pain Syndrome, Current Concepts and Treatment Options. Curr Pain Headache Rep. 2018;22(2):10.
9. Maleki J, et al. Patterns of spread in complex regional pain syndrome, type I (reflex sympathetic dystrophy). Pain. 2000;88(3):259–66.
10. Terkelsen AJ, et al. Bilateral hypersensitivity to capsaicin, thermal, and mechanical stimuli in unilateral complex regional pain syndrome. Anesthesiology. 2014;120(5):1225–36.
11. Veldman PH, et al. Signs and symptoms of reflex sympathetic dystrophy: prospective study of 829 patients. Lancet. 1993;342(8878):1012–6.
12. Yin C, et al. Transcriptome profiling of dorsal root ganglia in a rat model of complex regional pain syndrome type-I reveals potential mechanisms involved in pain. J Pain Res. 2019;12:1201–16. 10.2147/JPR.S188758.
13. Hu Q, et al. TRPV1 Channel Contributes to the Behavioral Hypersensitivity in a Rat Model of Complex Regional Pain Syndrome Type 1. Front Pharmacol. 2019;10:453.
14. Coderre TJ, et al. Chronic post-ischemia pain (CPIP): a novel animal model of complex regional pain syndrome-type I (CRPS-I; reflex sympathetic dystrophy) produced by prolonged hindpaw ischemia and reperfusion in the rat. Pain. 2004;112(1–2):94–105.

15. Chen R, et al. Expression profiling of spinal cord dorsal horn in a rat model of complex regional pain syndrome type-I uncovers potential mechanisms mediating pain and neuroinflammation responses. J Neuroinflammation. 2020;17(1):162.
16. Wang J, et al. Electroacupuncture Alleviates Mechanical Allodynia of a Rat Model of CRPS-I and Modulates Gene Expression Profiles in Dorsal Root Ganglia. Front Neurol. 2020;11:580997.
17. Jancalek R. Signaling mechanisms in mirror image pain pathogenesis. Ann Neurosci. 2011;18(3):123–7.
18. Choi HS, et al. Microglial interleukin-1beta in the ipsilateral dorsal horn inhibits the development of mirror-image contralateral mechanical allodynia through astrocyte activation in a rat model of inflammatory pain. Pain. 2015;156(6):1046–59.
19. Hu Q, et al., *Chronic Post-Ischemia Pain Model for Complex Regional Pain Syndrome Type-I in Rats*. J Vis Exp, 2020(155).
20. Chai W, et al. Electroacupuncture Alleviates Pain Responses and Inflammation in a Rat Model of Acute Gout Arthritis. Evid Based Complement Alternat Med. 2018;2018:2598975.
21. Chaplan SR, et al. Quantitative assessment of tactile allodynia in the rat paw. J Neurosci Methods. 1994;53(1):55–63.
22. Dixon WJ. Efficient analysis of experimental observations. Annu Rev Pharmacol Toxicol. 1980;20:441–62.
23. Chen W, et al. iRNA(m6A)-PseDNC: Identifying N(6)-methyladenosine sites using pseudo dinucleotide composition. Anal Biochem. 2018;561–562:59–65.
24. Subramanian A, et al. Gene set enrichment analysis: a knowledge-based approach for interpreting genome-wide expression profiles. Proc Natl Acad Sci U S A. 2005;102(43):15545–50.
25. Yin C, et al. Eucalyptol alleviates inflammation and pain responses in a mouse model of gout arthritis. Br J Pharmacol. 2020;177(9):2042–57.
26. Livak KJ, Schmittgen TD. Analysis of relative gene expression data using real-time quantitative PCR and the 2(-Delta Delta C(T)) Method. Methods. 2001;25(4):402–8.
27. Chung MK, et al., *Transcriptome analysis of trigeminal ganglia following masseter muscle inflammation in rats*. Mol Pain, 2016. 12.
28. Thakur M, et al. Defining the nociceptor transcriptome. Front Mol Neurosci. 2014;7:87.
29. Goswami SC, et al. Molecular signatures of mouse TRPV1-lineage neurons revealed by RNA-Seq transcriptome analysis. J Pain. 2014;15(12):1338–59.
30. Franceschini A, et al. STRING v9.1: protein-protein interaction networks, with increased coverage and integration. Nucleic Acids Res. 2013;41(Database issue):D808-15.
31. Shannon P, et al. Cytoscape: a software environment for integrated models of biomolecular interaction networks. Genome Res. 2003;13(11):2498–504.
32. Li Y, et al. Transcriptome profiling of long noncoding RNAs and mRNAs in spinal cord of a rat model of paclitaxel-induced peripheral neuropathy identifies potential mechanisms mediating

neuroinflammation and pain. J Neuroinflammation. 2021;18(1):48.
33. Xu X, et al. N-methyl-d-aspartate receptor subunit 2B on keratinocyte mediates peripheral and central sensitization in chronic post-ischemic pain in male rats. Brain Behav Immun. 2020;87:579–90.
34. Donnelly CR, et al. Central Nervous System Targets: Glial Cell Mechanisms in Chronic Pain. Neurotherapeutics. 2020;17(3):846–60.
35. Matsuda M, Huh Y, Ji RR. Roles of inflammation, neurogenic inflammation, and neuroinflammation in pain. J Anesth. 2019;33(1):131–9.
36. Chen R, et al. The NLRP3 inflammasome: an emerging therapeutic target for chronic pain. J Neuroinflammation. 2021;18(1):84.
37. Ji RR, Chamessian A, Zhang YQ. Pain regulation by non-neuronal cells and inflammation. Science. 2016;354(6312):572–7.
38. Du H, et al. Analyses of gene expression profiles in the rat dorsal horn of the spinal cord using RNA sequencing in chronic constriction injury rats. J Neuroinflammation. 2018;15(1):280.
39. Yin C, et al. IL-33/ST2 induces neutrophil-dependent reactive oxygen species production and mediates gout pain. Theranostics. 2020;10(26):12189–203.
40. Trevisan G, et al. TRPA1 mediates trigeminal neuropathic pain in mice downstream of monocytes/macrophages and oxidative stress. Brain. 2016;139(Pt 5):1361–77.
41. Zhang L, et al. Key role of CCR2-expressing macrophages in a mouse model of low back pain and radiculopathy. Brain Behav Immun. 2021;91:556–67.
42. Yu X, et al. Dorsal root ganglion macrophages contribute to both the initiation and persistence of neuropathic pain. Nat Commun. 2020;11(1):264.
43. Denk F, Bennett DL, McMahon SB. Nerve Growth Factor and Pain Mechanisms. Annu Rev Neurosci. 2017;40:307–25.
44. Dib-Hajj SD, et al. Rescue of alpha-SNS sodium channel expression in small dorsal root ganglion neurons after axotomy by nerve growth factor in vivo. J Neurophysiol. 1998;79(5):2668–76.
45. Zhang X, Huang J, McNaughton PA. NGF rapidly increases membrane expression of TRPV1 heat-gated ion channels. EMBO J. 2005;24(24):4211–23.
46. Jiang BC, Liu T, Gao YJ. Chemokines in chronic pain: cellular and molecular mechanisms and therapeutic potential. Pharmacol Ther. 2020;212:107581.
47. Wu XB, et al. CXCL13/CXCR5 enhances sodium channel Nav1.8 current density via p38 MAP kinase in primary sensory neurons following inflammatory pain. Sci Rep. 2016;6:34836.
48. Jiang BC, et al. CXCL13 drives spinal astrocyte activation and neuropathic pain via CXCR5. J Clin Invest. 2016;126(2):745–61.

Figures

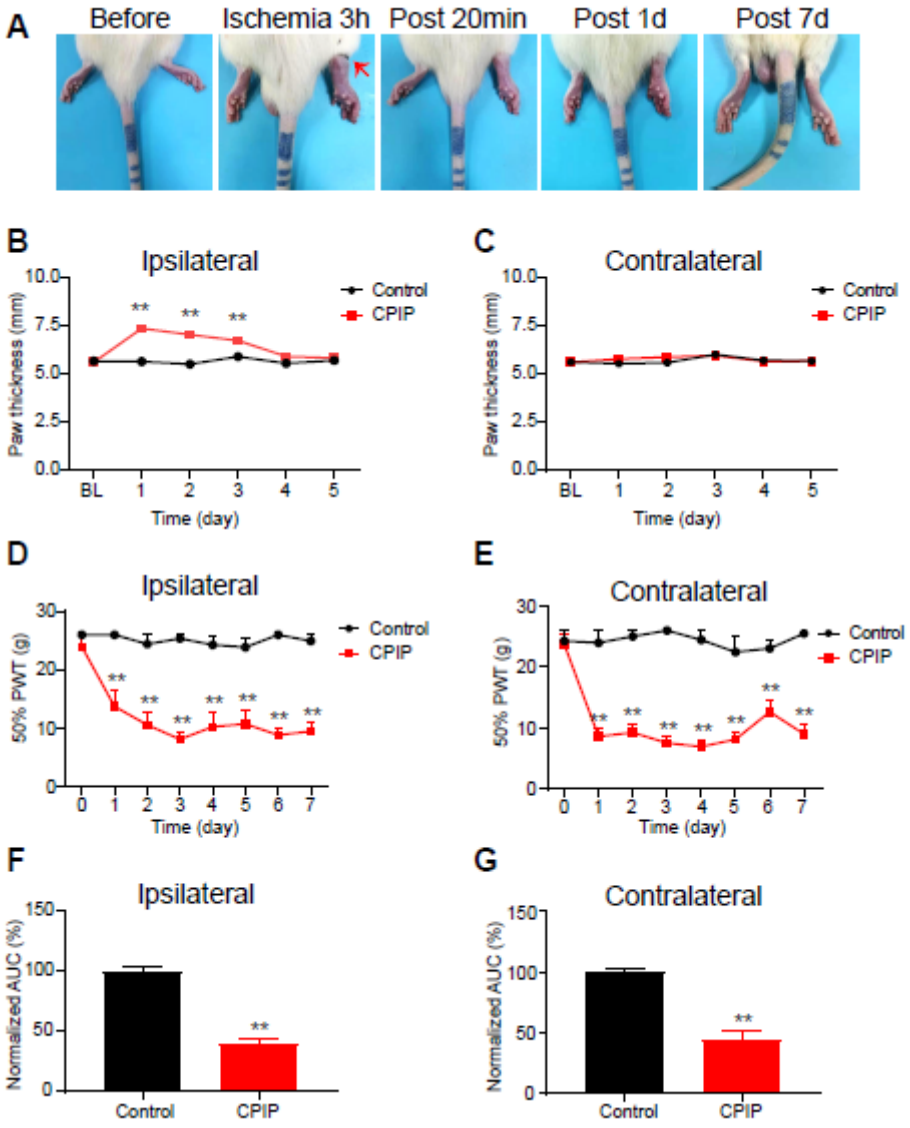

Figure 1

The CPIP model rats displayed remarkable and prolonged mechanical allodynia in both ipsilateral and contralateral hind paws. (A) Representative pictures of the rat hind paw taken before/during CPIP model establishment and 20 min, 1 d and 7 d after model establishment. The arrow indicates the position of the O-ring. (B&C) Edema evaluation of the ipsilateral (B) and contralateral (C) hind paw. (D&E) 50% paw withdraw threshold (PWT) of ipsilateral (D) and contralateral (E) hind paw. (F&G) Summary of the normalized area under the curve (AUC) as in panels D&E, respectively. n = 7-8 rats/group. **p < 0.01 vs. control group. Student's t-test or two-way ANOVA followed by Tukey post-hoc test was used for statistical analysis.

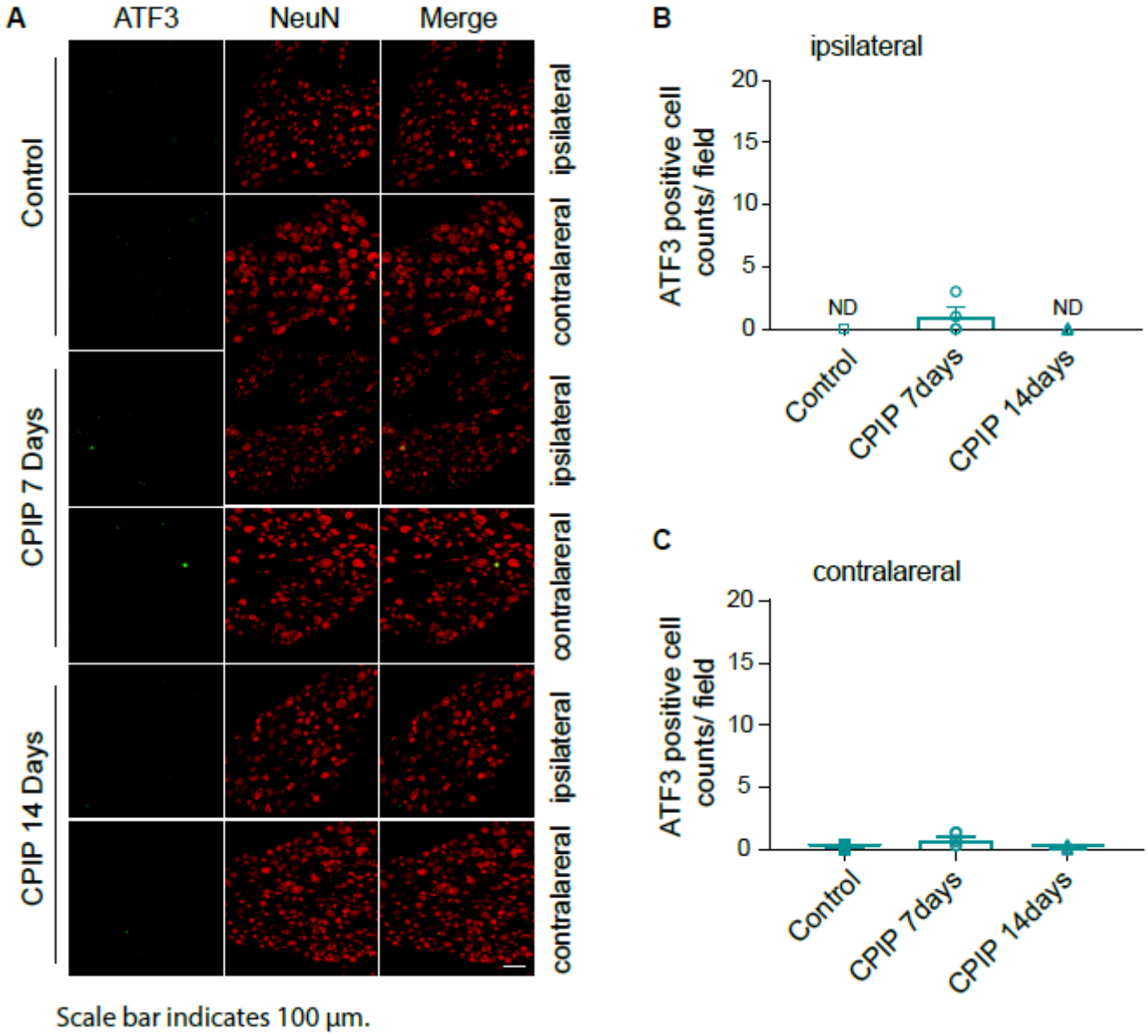

Figure 2

The CPIP model rats did not show any neuronal damage in bilateral DRG neurons innervating the hind limbs. (A) Representative immunostaining pictures showing ATF3 antibody (green) staining of ipsilateral and contralateral DRG from control group and CPIP model group. NeuN was used to label neurons (red). B. Summary of the number of ATF3 positive neurons per observation field in ipsilateral DRG. C. Summary of the number of ATF3 positive neurons per observation field in contralateral DRG. Scale bar indicates 100 µm. n = 4-5 rats/group.

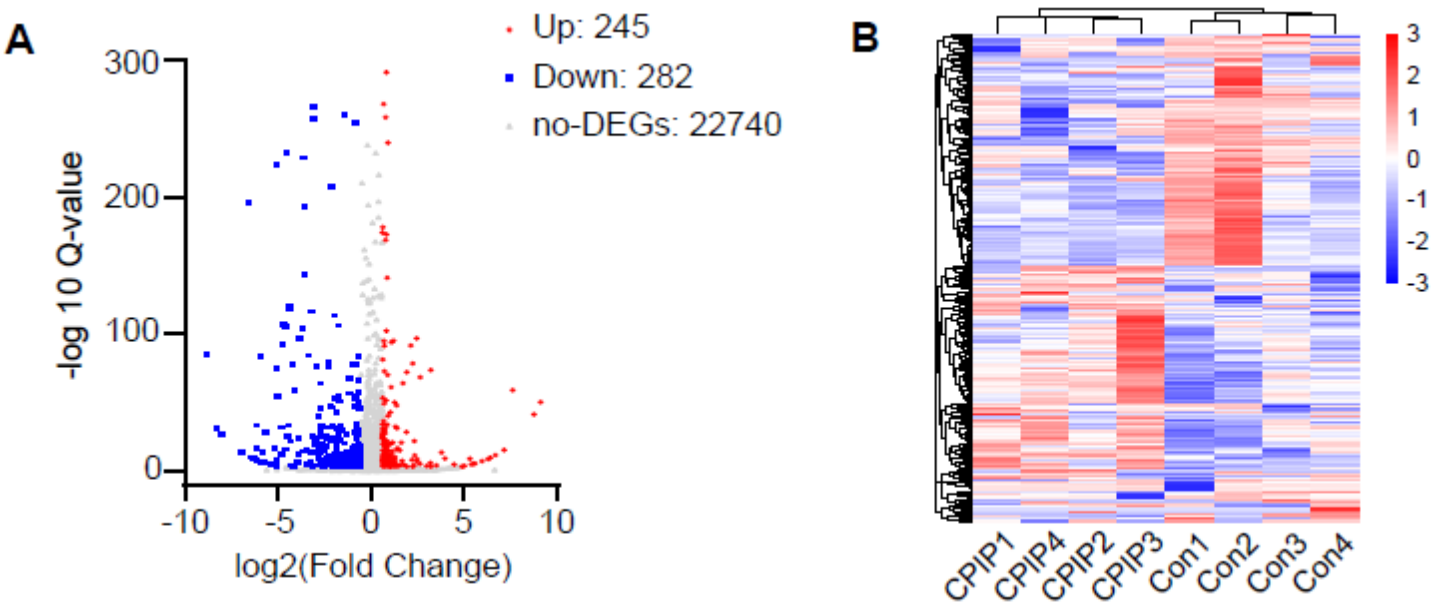

Figure 3

Gene expression profiling by RNA-Seq in contralateral DRG of CPIP model rats (A) Volcano plot illustrating gene expression profiles in contralateral DRG of CPIP model group vs. control group. Red and blue dots show up- and down-regulated DEGs, respectively. Gray dots indicate non-DEGs. (B) Heat map showing the hierarchical clustering of DEGs from CPIP and control groups and within groups.

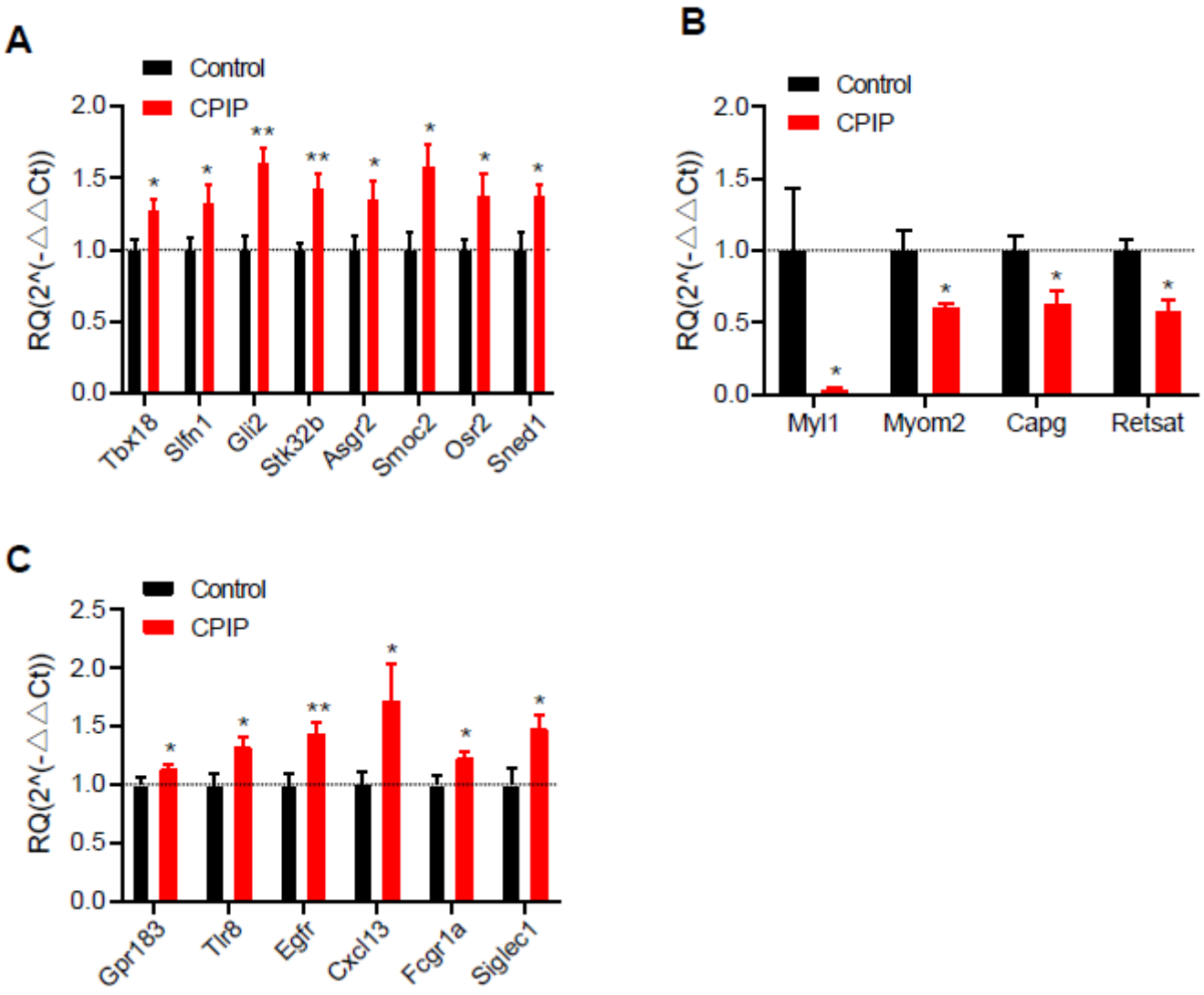

Figure 4

Validating the RNA-Seq results by means of qPCR. (A&B) qPCR validation of the expression of some randomly selected up-regulated (A) and down-regulated (B) DEGs from contralateral DRG. (C) qPCR validation of the expression of some representative genes involved in pain and neuroinflammation. n = 7 rats/group. *p < 0.05, **p < 0.01 vs. control group. Student's t test was used for comparisons.

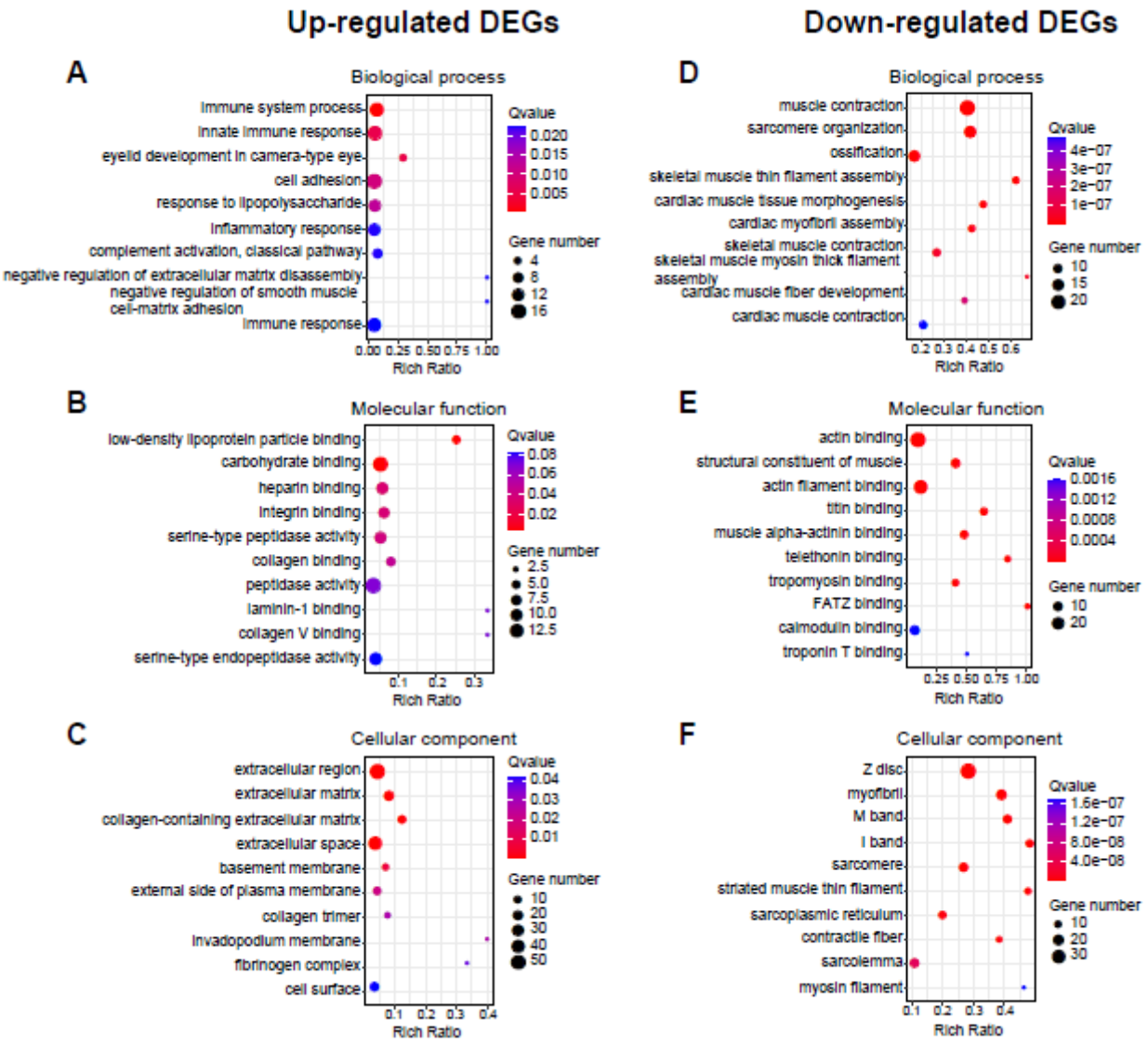

Figure 5

GO enrichment analysis of identified DEGs from contralateral DRG. (A-C) Bubble plots showing the top 10 mostly enriched biological processes, molecular functions and cellular components of up-regulated DEGs. (D-F) Bubble plots showing the top 10 mostly enriched biological processes, molecular functions and cellular components of down-regulated DEGs. Larger bubbles indicate higher number of genes and vice versa. The color of each bubble reflects the significance as indicated (q-value).

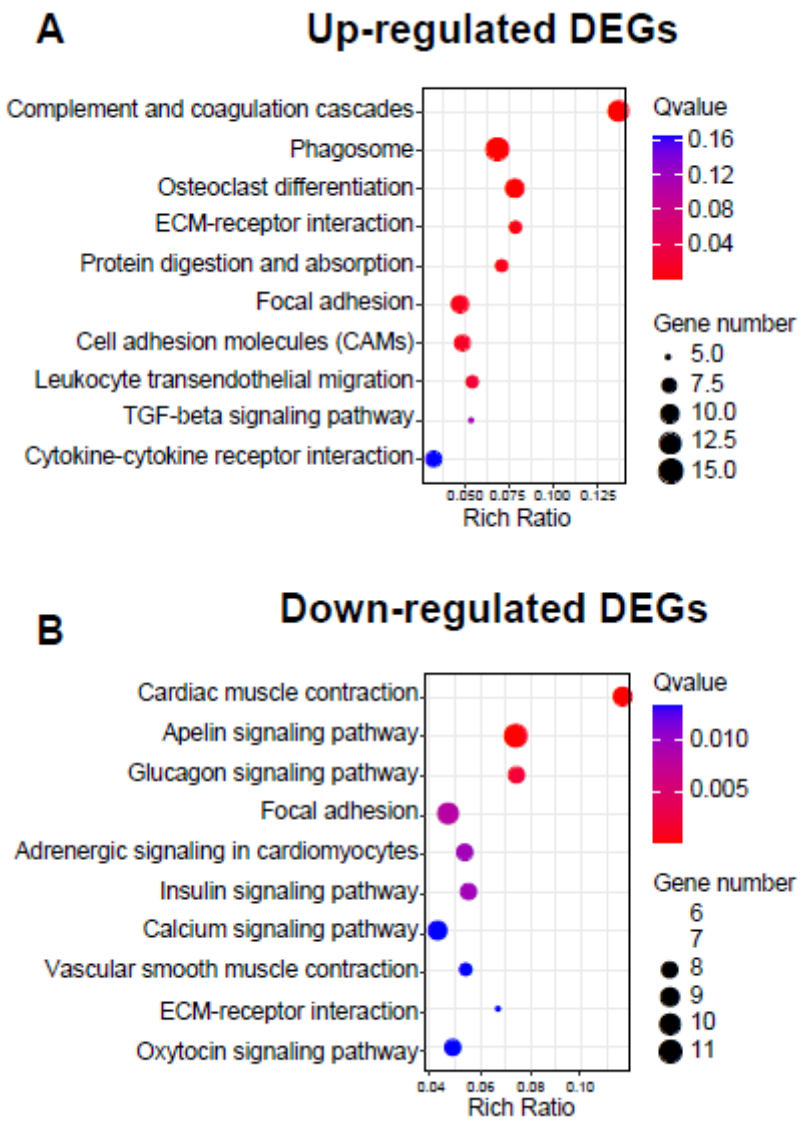

Figure 6

KEGG pathway analysis of identified DEGs from contralateral DRG. (A) Bubble plots showing the top 10 pathways of up-regulated DEGs identified by KEGG. (B) Bubble plots showing the top 10 pathways of down-regulated DEGs identified by KEGG. Larger bubbles indicate higher number of genes and vice versa. The color of each bubble reflects significance as indicated (q-value).

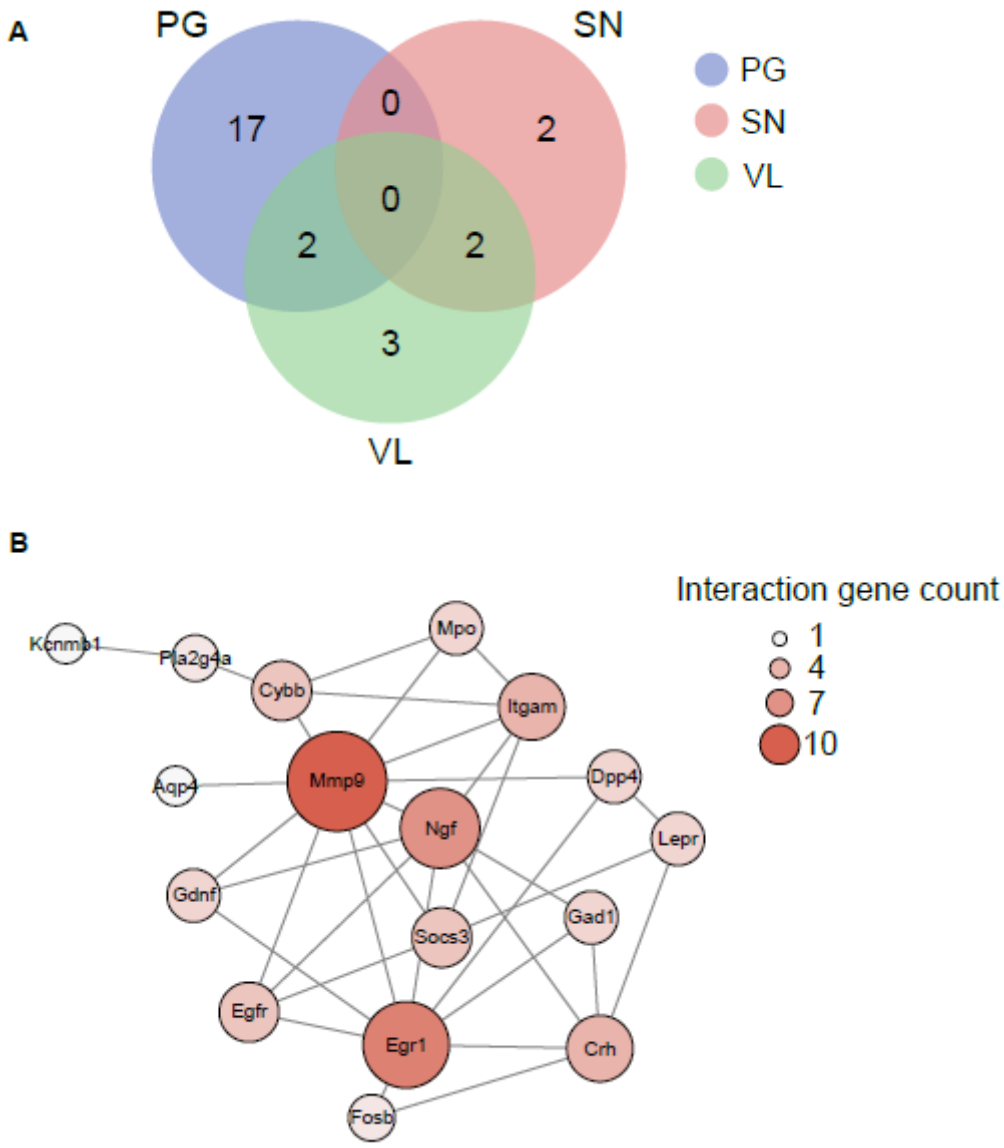

Figure 7

Analysis of DEGs potentially involved in pain mechanisms. (A) Overlapped DEGs with genes involved in pain processing (PG, in blue), genes enriched in TRPV1-lineage DRG neurons (VL, in green) and genes enriched in small-diameter DRG neurons (SN, pink) illustrated via Venn diagram. (B) The construction of PPI network of DEGs which showed overlapping with PG, VL and SN gene pools. Deeper color and larger circle indicate more protein-protein interactions and vice versa.

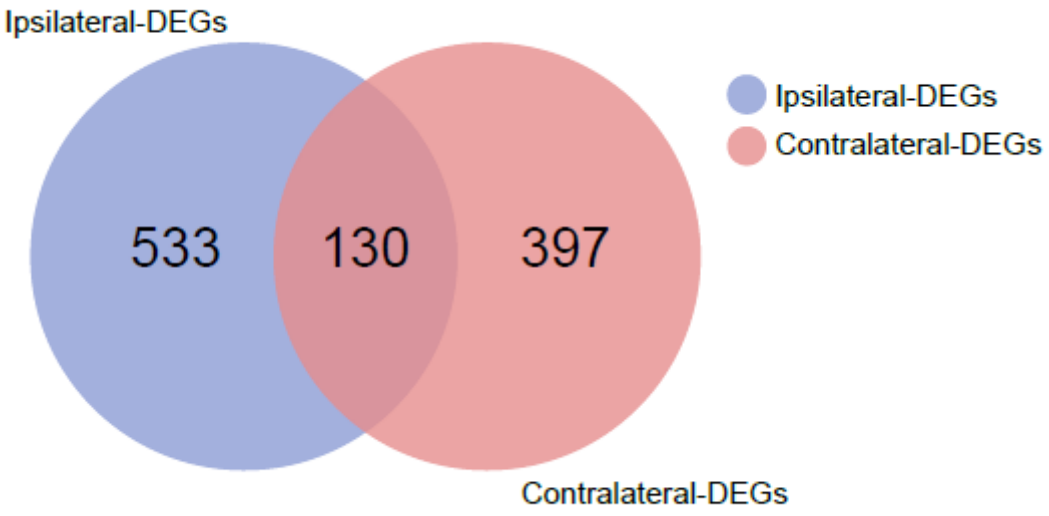

Figure 8

Comparison analysis of our current RNA-Seq dataset of contralateral DRG with that derived from ipsilateral DRG in CPIP model rats. Venn diagram illustration of the overlapped DEGs derived from contralateral and ipsilateral DRG RNA-Seq dataset.

Supplementary Files

This is a list of supplementary files associated with this preprint. Click to download.

- Suppl.Fig.1RIN.pdf
- Suppl.Fig.2GSEA.pdf
- Suppl.Table1CopyofHumanpaingenes.xlsx
- Suppl.Table2Genesenrochedinnociceptors.xlsx
- Suppl.Table3TRPV1lineagegenelist.xlsx
- Suppl.Table4Allgenes.xlsx
- Suppl.Table5AllDEGs.xlsx
- Suppl.Table6TheDEGsofGOanalysis.xlsx
- Suppl.Table7TheDEGsofKEGGanalysis.xlsx
- Suppl.Table8Thegenelistofoverlapping.xlsx
- Suppl.Table9TheoverlappingofbilateralDEGs..xlsx